Free Radicals Within the Antarctic Vortex: The Role of CFCs in Antarctic Ozone Loss

J. G. ANDERSON, D. W. TOOHEY, W. H. BRUNE

How strong is the case linking global release of chlorofluorocarbons to episodic disappearance of ozone from the Antarctic stratosphere each austral spring? Three lines of evidence defining a link are (i) observed containment in the vortex of ClO concentrations two orders of magnitude greater than normal levels; (ii) in situ observations obtained during ten high-altitude aircraft flights into the vortex as the ozone hole was forming that show a decrease in ozone concentrations as ClO concentrations increased; and (iii) a comparison between observed ozone loss rates and those predicted with the use of absolute concentrations of ClO and BrO, the rate-limiting radicals in an array of proposed catalytic cycles. Recent advances in our understanding of the kinetics, photochemistry, and structural details of key intermediates in these catalytic cycles as well as an improved absolute calibration for ClO and BrO concentrations at the temperatures and pressures encountered in the lower antarctic stratosphere have been essential for defining the link.

DURING THE LAST DECADE THERE HAS BEEN CONSIDERable growth in our understanding of the linkage among biological, chemical, and physical processes that interactively establish both the chemical composition of the atmosphere, ocean, and terrestrial domain, as well as the climate. Behind this evolving understanding of the network of dissimilar processes resides a growing body of experimental data that has led to increasing success in relating cause and effect.

Many examples of significant global-scale change have emerged during the last decade (*1*), and one of the most important has been the discovery by Farman and co-workers (*2*) of episodic O_3 loss each austral spring over the Antarctic continent. Building on 25 years of nearly continuous O_3 column-density measurements from the British Antarctic Survey station at Halley Bay (77°S latitude), Farman began to detect brief periods of O_3 decline extending over a 6-week period following the return of solar illumination each spring. Although the effect was subtle in the late 1970s, the signature strengthened through the 1980s such that by 1984 ozone depletion levels reached 30% in the October monthly mean values. Announcement of these observations in 1985 (*2*) led immediately to a complete mapping of the recurring and worsening event with the use of archived satellite data (*3*). The mapping revealed that O_3 loss was occurring in a region the size of the Antarctic continent commensurate with losses reported from Halley Bay. In the 4 years since, O_3 levels have continued to drop such that in 1989 70% of the total column O_3 content over the Antarctic continent (*4*) (10% of the area of the Southern Hemisphere) was lost during the month of September and early October. This precipitous loss of 3% of the world's O_3 in a period of 6 weeks graphically illustrates how rapidly global-scale atmospheric changes can occur. In this article we describe observational data that pertain to a single issue: the case linking chlorofluorocarbons (CFCs) to the observed loss of O_3 in the Antarctic vortex. The central question is whether we can establish the causal link between surface release of CFCs and the massive loss of O_3 in the Southern Hemisphere.

Theories to explain the cause of Antarctic O_3 depletion blossomed after its discovery. On the basis of the highly layered distribution of O_3, which peaks at 19 km over Antarctica, dynamical theories held that vertical advection driven by solar heating was responsible (*5*). Detailed calculations coupling these dynamical processes to quantitative predictions of O_3 loss from the vortex remained elusive, but there was an inherent simplicity in the concept of vertical motion displacing the O_3 layer vertically or horizontally, thereby bringing in O_3-poor air from the upper troposphere. Another class of theories surfaced that was in various forms tied to events external to Earth. Callis *et al.* (*6*) suggested that solar proton events could increase the production rate of nitrogen oxides in the polar region; NO and NO_2 are chain-carrying radicals in the chemical catalysis of O_3. Finally, there was the class of theories abstracted from the concept put forward in 1974 by Molina and Rowland (*7*) that related Cl radicals to global O_3 loss through chemical catalysis, specifically in the reaction couplet

$$Cl + O_3 \rightarrow ClO + O_2$$

$$\underline{ClO + O \rightarrow Cl + O_2}$$

$$\text{Net: } O_3 + O \rightarrow O_2 + O_2$$

Three variations on halogen free-radical catalysis emerged to explain the observations by Farman and co-workers. First, Molina and Molina (*8*) suggested that a ClO dimer was involved in a quartet of reactions (Mechanism I):

$$ClO + ClO + M \xrightarrow{k_1} (ClO)_2 + M$$

$$(ClO)_2 + h\nu \rightarrow Cl + ClOO$$

$$ClOO + M \rightarrow Cl + O_2 + M$$

$$\underline{2 \times (Cl + O_3 \rightarrow ClO + O_2)}$$

$$\text{Net: } 2O_3 \rightarrow 3O_2$$

where $h\nu$ designates an ultraviolet photon and M signifies a collisional chaperone, either N_2 or O_2, and k is the pressure- and

J. G. Anderson and D. W. Toohey are in the Department of Chemistry and Department of Earth and Planetary Sciences, Harvard University, Cambridge, MA 02138. W. H. Brune is in the Department of Meteorology, Pennsylvania State University, University Park, PA 16802.

temperature-dependent rate constant of the rate-limiting step. The presence of radical-radical recombination to form structures bound by 10 to 20 kcal/mol, as exemplified by this mechanism, has implications for catalysis in general: for low-temperature regions of Earth's atmosphere this process opens up important photochemical channels that are as yet unexplored. Secondly, McElroy *et al.* (*9*) suggested that chlorine and bromine are coupled in O_3 destruction through a three-step sequence (Mechanism II):

$$ClO + BrO \xrightarrow{k_2} Cl + Br + O_2$$

$$Cl + O_3 \rightarrow ClO + O_2$$

$$\underline{Br + O_3 \rightarrow BrO + O_2}$$

$$\text{Net: } 2O_3 \rightarrow 3O_2$$

Finally, Solomon *et al.* (*10*) suggested that Cl and H radicals are coupled in the sequence (Mechanism III)

$$HO_2 + ClO \xrightarrow{k_3} HOCl + O_2$$

$$HOCl + h\nu \rightarrow OH + Cl$$

$$Cl + O_3 \rightarrow ClO + O_2$$

$$\underline{OH + O_3 \rightarrow HO_2 + O_2}$$

$$\text{Net: } 2O_3 \rightarrow 3O_2$$

These theories reflect the realization that O atoms could not be involved quantitatively in O_3 destruction because the concentration of O atoms was too low in the polar stratosphere. The concentration is reduced there because of both the lack of ultraviolet radiation in late winter and the greater atmospheric density at the O_3 concentration peak, which is ~7 km lower in altitude in the polar regions than at midlatitudes. For completeness, however, we also consider the contribution to O_3 destruction by the original Rowland and Molina mechanism, which is rate limited by the reaction (Mechanism IV)

$$ClO + O \xrightarrow{k_4} Cl + O_2$$

Other theories too numerous to mention never made it beyond the popular press.

The first concerted experimental effort to evaluate these theories was the National Science Foundation National Ozone Experiment (NOZE I) expedition in the austral spring of 1986. This project collected ground-based spectroscopic data in the near ultraviolet, visible, middle-infrared, and millimeter-wave regions and balloon-borne, in situ O_3, particle, and temperature data. A great deal was learned from that expedition: (i) balloon sondes showed the time and altitude dependence of O_3 loss and revealed that O_3 was almost completely removed by the beginning of October in the core of the O_3 layer (*11*); (ii) the ground-based, near ultraviolet–visible spectrometer showed that OClO column densities were elevated by more than an order of magnitude over those obtained at midlatitude (*12*) and that NO_2 column concentrations were low (*13*); (iii) millimeter-wave emission data showed that ClO densities in the vicinity of 20 km were elevated (*14*); and (iv) high-resolution, middle-infrared column measurements of $ClONO_2$ and HCl concentrations provided strong evidence that chlorine chemistry was perturbed (*15*).

Taken collectively, the NOZE I results substantiated the premise that the vortex was highly perturbed chemically and that hitherto more intuitively appealing dynamical theories were not without serious challenge. At the same time, it became clear that whatever specific mechanism was responsible for the removal of O_3 from the vortex region, the stage for redistribution or destruction was set by strong diabatic cooling of the vortex core through the polar winter, coupled with isolation of the region from heat and momentum flux supplied from mid and low latitudes.

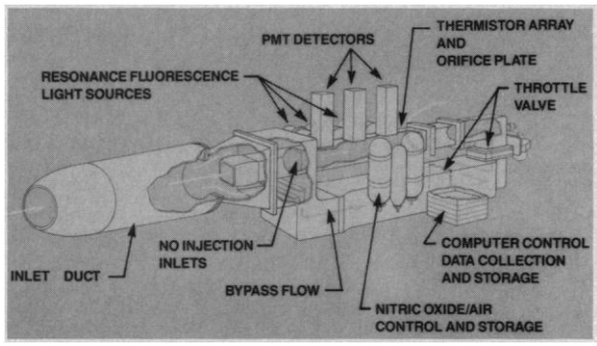

Fig. 1. Perspective of the instrument architecture showing the double-ducting geometry used to both maintain laminar flow and decelerate the flow from 200 to 15 m s^{-1}. The inlet duct extracts unperturbed air from in front of the left wing pod and drops the flow velocity to 60 m s^{-1}; a second duct extracts the laminar core from that flow and drops the flow velocity to 15 m s^{-1} through three tandem optical axes. ClO is converted to Cl by the rapid bimolecular reaction $ClO + NO \rightarrow Cl + NO_2$, and the product Cl atom is detected by atomic resonance scattering. The analogous reaction is used for BrO. The instrument is 1.5 m in length.

With an eye on establishing the mechanism for O_3 removal, a joint NASA-NOAA-NSF-CMA expedition was organized (*16*) in which aircraft were used to obtain both in situ data in the vortex at the approximate altitude of the O_3 concentration peak and survey data from immediately below the O_3 layer from remote-sensing instruments and lidar. The NASA ER-2 and DC-8 aircraft platforms were used respectively for these observations. The subset of the AAOE data that directly addressed the role of CFCs in Antarctic O_3 destruction was the in situ detection of halogen radicals from the ER-2 aircraft.

The Experiment

In situ detection of part-per-trillion levels of ClO and BrO in the stratosphere was achieved before the discovery of the Antarctic O_3 hole. In the detection method, a flowing sample is extracted from the atmosphere, and ClO and BrO are chemically converted to Cl and Br by the rapid bimolecular reaction ClO (BrO) + NO → Cl (Br) + NO_2. Then, atomic-resonance scattering, with the use of allowed electronic transitions in the vacuum ultraviolet, is used to determine the Cl and Br concentration. The high-intensity, spectrally pure emission used to induce atomic-resonance scattering by the halogen atoms contained in the atmospheric sample is obtained from Cl (Br) atoms in a low-pressure He plasma sustained by a 180-MHz field confined in a cylindrical quartz envelope with magnesium fluoride windows.

For application of this technique to aircraft observations, significant changes were made. The instrument has a double-ducted architecture (Fig. 1) to provide control of the flow through the tandem optical axes used to detect ClO and BrO (*17*). Specifically, the objective was to decelerate the 200 m s^{-1} flow from the aircraft free stream to approximately 15 m s^{-1} in order to facilitate time-resolved chemical conversion of ClO to Cl. At the same time, laminar flow with confined boundary-layer growth was essential because radicals, like ions, are destroyed by collision with instrument walls.

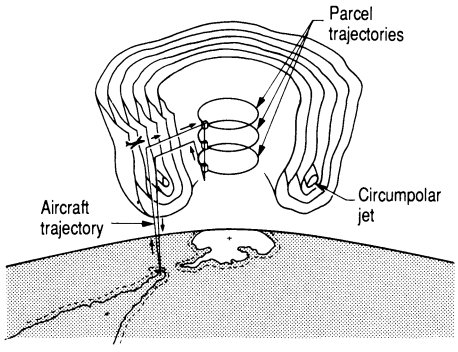

Fig. 2. Spatial relationship of the South American and Antarctic continents, the circumpolar wind field, the aircraft trajectories, and parcel trajectories.

There were two components to the calibration. In the laboratory phase, the tandem optical axes (Fig. 1) were removed from the flight instrument and vacuum sealed into a flow reactor that provided a high-velocity flow of $N_2 - O_2$ mixtures at the appropriate temperature, pressure, and velocity encountered during flight. That flow was seeded with a known concentration of Cl or Br (<10 ppb) determined with atomic absorption spectroscopy. For a given absolute concentration of the atom, the count rate of the instrument detector that resulted from atomic resonance scattering was determined simultaneously with the partial derivative of the Rayleigh-scattering signal as a function of the N_2/O_2 concentration. In the airborne phase, the slope and intercept of the concentration-dependent Rayleigh scatter was analyzed at the midway point of each flight when the aircraft descended rapidly from 18.5 km to 13 km and then returned to altitude (*18*).

Ozone was detected by its absorption of 254-nm light from a mercury resonance lamp. Two absorption chambers that alternately sampled ambient and O_3-scrubbed air were used. For an integration time of 1 s, the detection limit was 0.5 to 1.0 ppbv at standard temperature and pressure. The accuracy for O_3 concentration is ±5% (*19*).

The Mission

Mission strategy (*16*) was to employ the medium-range (6000 km), high-altitude (19 km) ER-2 reconnaissance aircraft with the long-range (10,000 km), medium-altitude (11 km) DC-8 aircraft in an organized investigation of the Antarctic vortex region. Several scientific questions dominated the selection of a canonical ER-2 trajectory: If spatial or temporal changes in O_3 are detected, can the effects of chemistry and dynamics be separated? What is the structure of O_3 depletion? What is the extent, temperature dependence, size distribution, and chemical composition of particulate matter in the vortex? What are the spatial and temporal relations of O_3 concentrations with those of reactive halogen and nitrogen compounds and with the abundance of polar stratospheric clouds? Is there sufficient ClO to sustain a rapid enough (when compared to observed O_3 loss) non-O atom catalytic chain? What is the extent of BrO involvement?

The adopted flight trajectory (Fig. 2) represented the maximum penetration distance afforded by performance and safety limitations of the ER-2 aircraft: rapid ascent from Punta Arenas, Chile (54°S), to 18 km, adherence to a constant potential-temperature, θ (*20*), surface to 72°S, a rapid descent-ascent sequence to and from 13 km, a homeward leg on a fixed potential-temperature surface, and descent into Punta Arenas. Following two flights on 17 and 18 August, which were truncated by temperatures at altitude below the operating threshold of the ER-2 (−85°C), a series of ten flights was executed commencing on 23 August and ending on 22 September 1987.

Adherence to a surface of constant θ on a given trajectory was important because θ is a conserved quantity in any adiabatic process. Even though diabatic processes were important during the polar winter, through the 4-week period covered by the experiments intravortex motion was virtually adiabatic (*21*). Atmospheric variability resulting from vertical displacements is suppressed in an isentropic (constant θ) reference frame. Typically, the ER-2 adhered to either the 450 K or 425 K surface on the southbound and northbound legs and scanned from 450 K (~18.5 km) to 350 K (~13 km) during dive segments.

The full data scan for the 23 August flight (Fig. 3), from the time the aircraft reached altitude just south of Punta Arenas on the southbound leg to a point just before descent into Punta Arenas on the northbound leg, is representative of the data collected on all ten flights. The observations showed that equatorward of the vortex edge, ClO mixing ratios at altitude can be as low as those typically observed at mid-latitude (2 to 5 parts per trillion by volume, pptv). These are easily observed ClO mixing ratios because the detection threshold of the instrument is 1 pptv for a 2-min integration time. The measured ClO mixing ratios exhibited a sharp transition poleward of the vortex edge and reached levels in the vortex more than two orders of magnitude higher than those observed outside the vortex. A dramatic vertical gradient in ClO mixing ratios is evident in the data from the southernmost descent-ascent sequence

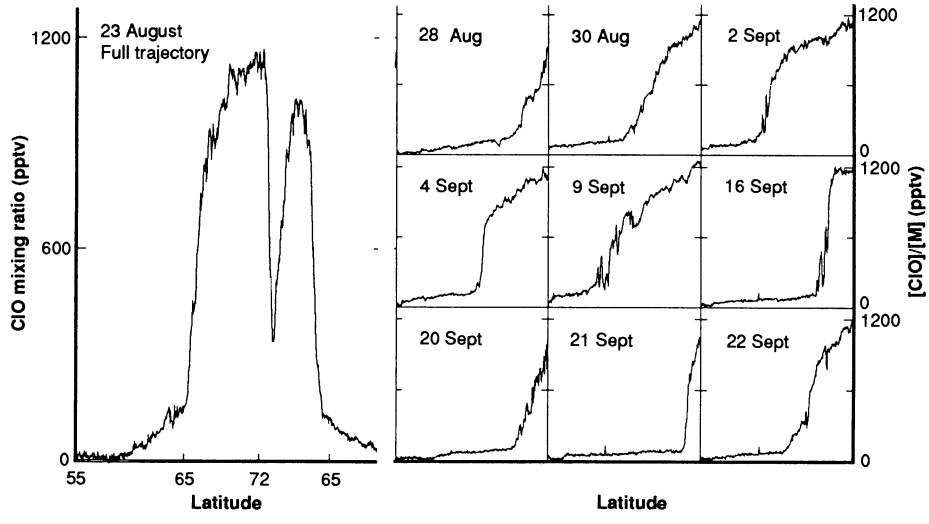

Fig. 3. Summary of the ClO data obtained on the ten ER-2 flights into the vortex, which followed the trajectory displayed in Fig. 2. (**Left**) The full trajectory from the point above Punta Arenas where the aircraft reached cruise altitude (~18 km), through the southbound leg to 72°S, the descent-ascent sequence, and the northbound leg. (**Right**) Southbound segment of the flight trajectories (55° to 72°) for the remaining nine missions.

at 72°S latitude (Fig. 3).

Companion measurements obtained with instruments on board the ER-2 demonstrated that the region in which ClO was so dramatically amplified was sharply depleted in nitrogen oxides and nitric acid (*22*), was suppressed in those tracers originating in the troposphere (*23*), was markedly depleted in water vapor (*24*), and, in the latter part of August, contained O_3 concentrations suppressed by ~15% relative to those observed in a band 10° in latitude equatorward of the ClO edge (*25*). The sharp gradient in ClO thus defines the position of a chemically perturbed region (CPR), the contents of which strongly support the concept that ice particles initially seeded by nitric acid trihydrate (NAT) convert HCl and $ClONO_2$ to Cl_2 and $HONO_2$ (*26*) (Fig. 4).

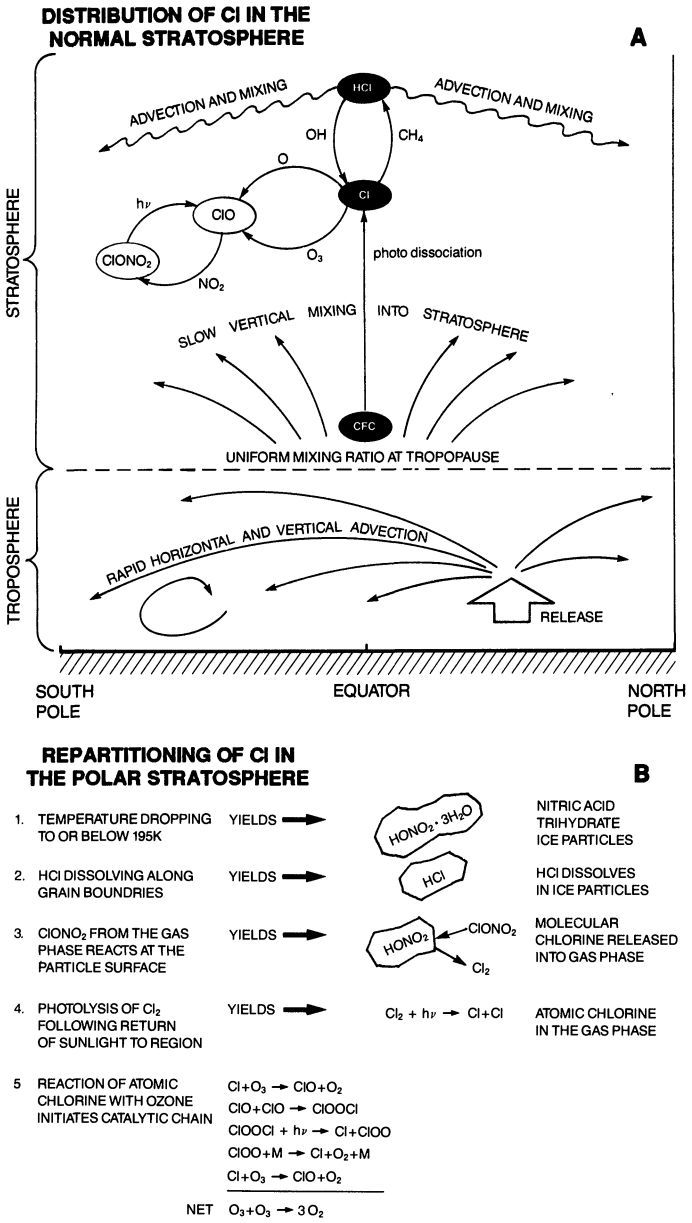

Fig. 4. (A) Schematic representation of the normal distribution of chlorine compounds in the stratosphere augmented by CFC release. This sequence of slow upward mixing of CFCs, photodissociation, and sequestering, primarily in the form of HCl and $ClONO_2$, results in a uniform mixing ratio of chlorine in any volume element of the stratosphere. (**B**) Heterogeneous processes taking place in the Antarctic vortex that are responsible both for the elimination of reactive nitrogen from the chemically perturbed region and for the subsequent repartitioning of chlorine from the dominant reservoir species, HCl and $ClONO_2$, to free-radical form, initiating the catalytic conversion of O_3 to O_2.

This process is summarized as follows (Fig. 4A): The global source of stratospheric chlorine is now dominated by CFC release at ground level; mixing processes in the troposphere rapidly distribute those CFCs globally. Slow vertical transport carries the compounds to the middle stratosphere on a time scale of decades, where they are photolytically decomposed. Mixing processes in the stratosphere ensure that the mole fraction of chlorine atoms (chemically bound or free) is, to first order, independent of altitude, latitude, and longitude in the stratosphere.

Several processes may be responsible for repartitioning chlorine from its stable reservoir species, HCl and $ClONO_2$, to the catalytically active forms, Cl and ClO (Fig. 4B). Specifically, NAT particles grow to sizes 1 to 3 μm in diameter, HCl is adsorbed onto the grain boundaries, and subsequent collisions with $ClONO_2$ liberate Cl_2 into the gas phase and tie up $HONO_2$ in the ice structure

$$ClONO_2(g) + HCl(s) \rightarrow Cl_2(g) + HONO_2(s)$$

These processes have been studied in laboratory experiments (*27*). Through the polar night as the entire core of the vortex diabatically cools and descends, precipitation of crystals containing nitric acid to lower altitudes effectively removes both water vapor and the photochemical source for nitrogen oxides. Gas-phase Cl_2 remains in the vortex. The Cl_2 is extremely unstable in the presence of ultraviolet light and dissociates in a matter of hours following exposure to sunlight. Thus, photolysis, $Cl_2 + h\nu \rightarrow Cl + Cl$, initiates the catalytic sequences (Mechanisms I to IV).

Data from the southbound leg of the 23 August flight trajectory establishes a baseline comparison with the other flights in the sequence (Fig. 5). Data from the nine additional flights reveal that (i) the variation of ClO observed on the flight of 23 August remained consistent to first order through the flight series; (ii) chlorine monoxide gradients at the CPR edge remained undiminished and showed signs of steepening through late September; (iii) peak ClO mixing ratios remained virtually constant at 1200 pptv from late August to late September for cases in which the aircraft penetrated the chemically perturbed region by 5° latitude or more; and (iv) the edge of the CPR migrated back and forth between latitudes of 64° and 71°S in response to the movement of synoptic-scale storm systems.

CFC-Ozone Case

Isolation of the chemically perturbed region. The first element in the case linking CFC release to Antarctic O_3 depletion hinges on the containment created by the circumpolar jet that defines the perimeter of the Antarctic vortex. This containment has both a physical and a chemical component. Typical wind fields at cruise altitude (*16, 28*) of the ER-2 exhibited remarkable azimuthal symmetry with the center of rotation nearly coincident with the geographic South Pole. Peak winds of 50 to 100 m s^{-1} (100 to 200 knots) were found in a latitude band from approximately 50° to 65°S. A region of restricted horizontal mixing characterized the region in a collar spanning 10° in latitude poleward of the peak wind field.

An analysis by Schoeberl and Hartmann (*21*), obtained by comparing the Arctic and Antarctic vortices, demonstrates several important features. First, containment occurs over a wide interval in latitude, where surfaces of constant θ are quasi-orthogonal to surfaces of constant potential vorticity (another conserved quantity in frictionless, adiabatic systems). Second, the region of high ClO is coincident with the volume in which the temperature is low enough to initiate a phase transition forming NAT particles. Thus, the size

of the inner vortex, the CPR, is determined by temperature, whereas the size of the outer vortex is determined by the wind field. Evidence for the isolation provided by this physical confinement is the steep gradient in ClO concentration observed by the aircraft along surfaces of constant θ (Fig. 3).

In this CPR a gradient in the concentration of the ClO radical is maintained over a dynamic range previously observed only in laboratory systems; furthermore, the concentration of the free radical is of such magnitude in the vortex that the characteristic time for O_3 loss by gas-phase homogeneous catalysis is short compared with the time constant for vertical exchange across surfaces of constant θ. In other words, in any volume element poleward of the ClO ledge, photochemical loss rates of O_3 significantly exceed flux divergence. Thus the continuity equation for O_3

$$d[O_3]/dt = P - L - \nabla\cdot\phi$$

where P and L are the O_3 photochemical production and removal terms, respectively, and $\nabla\cdot\phi$ is the flux divergence resulting from atmospheric motion, can be closely approximated by the expression

$$d[O_3]/dt \approx P - L$$

In addition, because the rate of O_3 production, P, is limited by the rate of O_2 photolysis, it can be shown that the loss rate, L, which is

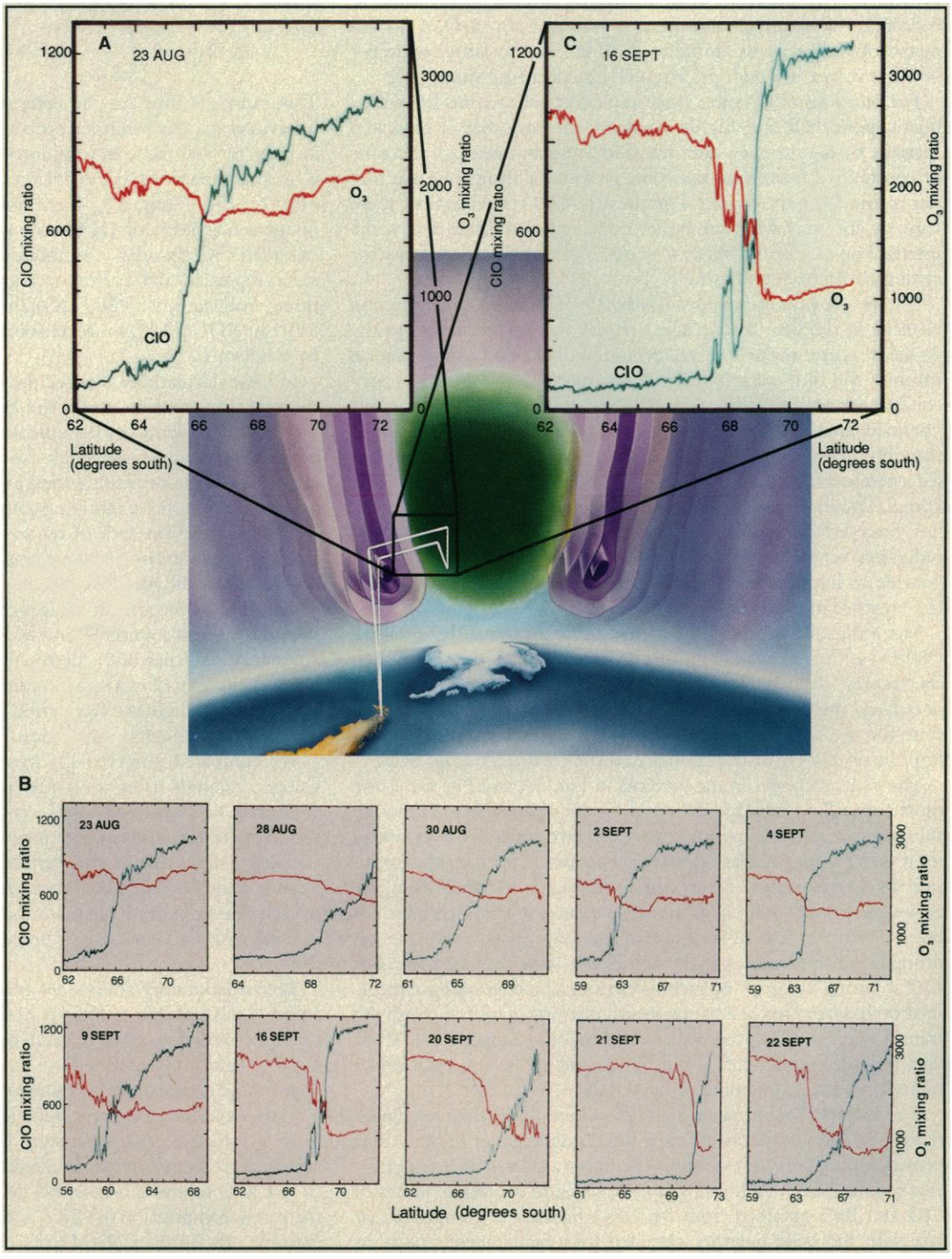

Fig. 5. Rendering of the containment provided by the circumpolar jet that isolates the region of highly enhanced ClO (shown in green) over the Antarctic continent. Evolution of the anticorrelation between ClO and O_3 across the vortex transition is traced from (**A**) the initial condition observed on 23 August 1987 on the southbound leg of the flight. (**B**) Summary of the sequence over the ten-flight series; (**C**) imprint on O_3 resulting from 3 weeks of exposure to elevated levels of ClO. Data panels do not include dive segment of trajectory; ClO mixing ratios are in parts per trillion by volume; O_3 mixing ratios are in parts per billion by volume.

equal to the sum of the rate-limiting steps in mechanisms I to IV, exceeds P by several orders of magnitude (*29*) during the course of this experimental series. Thus, the time rate of change of O_3 for the 23 August to 22 September 1987 period reduces to

$$d[O_3]/dt \approx L$$

on surfaces of constant θ.

Neglect of the flux-divergence term leads to the question of whether dynamical exchange of mass across the vortex edge can occur, particularly poleward of the ClO ledge, which lies well inside the vortex defined by meteorological variables (*30*). We concur with the conclusion of Schoeberl and Hartmann (*21*) that advective exchange of material in the region of the ER-2 dive (~7° poleward of the ClO ledge and 15° poleward of the polar jet core) will enhance demands placed on in situ chemical loss by at most 20%. However, collection of simultaneous, in situ tracer, ClO, BrO, O_3, and meteorological data to altitudes of 30 km and to latitudes deeper into the vortex is a high priority on subsequent missions.

For purposes of isolating cause and effect, we are thus left with a highly perturbed and highly confined air mass that is separated spatially by an extremely thin transition region. Although the zone of constrained horizontal transport provides a semipermeable barrier maintaining the dramatic gradient in ClO concentration, there may, of course, have been earlier exchange of material across the interface on time scales of a few weeks. The elements are in place for testing chemical hypotheses.

The development of anticorrelation between ClO and O_3. The second element in the case linking CFC release to O_3 destruction in the Antarctic vortex is the observed evolution of O_3-ClO anticorrelation through the time period spanned by the ten ER-2 flights. Initial conditions were established on 23 August 1987 when the aircraft obtained simultaneous observations of ClO and O_3 concentrations through the transition region (Fig. 5A). Although there is evidence for a reduction of ~15% in the O_3 concentration poleward of the vortex edge in these data (*31*), the first-order observation is that O_3 has emerged from the polar night without suffering dramatic reduction across the CPR transition. These data thus (Fig. 5A) provide an initial basis to interpret the temporal evolution of O_3 in the presence of enhanced levels of ClO.

The mission series yielded a ten-frame sequence of evolving ClO-O_3 anticorrelation (Fig. 5B). A monotonic decrease in O_3 in the "beaker" defined by the ClO ledge is evident on inspection of the data from the ten-flight sequence. Three weeks provides adequate time for the spatial distribution of ClO to leave an unmistakable imprint on the O_3 distribution across the CPR edge (Fig. 5C).

The contrast between the patterns in Fig. 5A and Fig. 5C is the most compelling message delivered by the observations. Although the presence of anticorrelation between two variables does not in itself prove a causal relation, the data sequence tracking the evolution of O_3 depletion (in a contained region isolated from the atmosphere as a whole) from an initial condition in which there has been a marginal loss of ozone to a condition in which ozone has dropped precipitously spatially coincident with amplified levels of ClO is strong evidence of such a relation. The developing anticorrelation has been tracked by the in situ instrumentation through the transition region on spatial scales equal to, or less than, 1 km. These data provide discrimination that is difficult to achieve even under carefully controlled laboratory conditions.

The kinetics of ozone destruction by halogen radical catalysis. Quantitative analysis of the mechanism for O_3 destruction in the vortex provides a final line of evidence. We have calculated the rate of O_3 loss resulting from each catalytic cycle using in situ observations of ClO and BrO obtained from the ER-2 flights and compared that rate with the same quantity obtained from simultaneous observations of O_3. Time rate of change of O_3 resulting from each of the catalytic processes (Mechanisms I to IV) is equal to the rate-limiting step in each cycle. For example, Mechanism I will destroy O_3 in a given volume element at a rate twice that of the slowest step in the catalytic quartet (because two O_3 molecules are destroyed each time the cycle is completed). Thus for Mechanism I

$$-(d[O_3]/dt) = 2k_1[ClO]^2_{obs}$$

where $[ClO]_{obs}$ is the experimentally determined free-radical concentration.

Integration of this equation over a 24-hour period yields the amount of O_3 removed in each diurnal cycle, which in turn can be set equal to the product of the square of the observed ClO concentration and an effective exposure time, Δt^I_{exp}, for each mechanism:

$$\Delta[O_3] = 2\int_{24\ hours} k_1[ClO]^2 dt = 2k_1[ClO]^2_{obs}\,\Delta t^1_{exp}$$

This exposure time can be determined accurately by solving the ultraviolet radiative-transfer problem for solar zenith angles in the vicinity of 90° (*32*), in conjunction with an appropriate set of elementary reactions that define the shape of the diurnal dependence of [ClO] (*29*). Thus, Δt^1_{exp} is the time period calculated to relate the integrated amount of O_3 removed in each diurnal cycle with the observed ClO abundance at noon, $[ClO]_{obs}$. Equally simple expressions represent the corresponding O_3 loss terms for the other three mechanisms: $2k_2[ClO][BrO]\Delta t^{II}_{exp}$ for Mechanism II; $2k_3[ClO][HO_2]\Delta t^{III}_{exp}$ for Mechanism III; and $2k_4[ClO][O]\Delta t^{IV}_{exp}$ for Mechanism IV.

In these calculations, we used the observed azimuthal symmetry of the trajectory motion about the geographic South Pole, coupled with the short period of latitudinal wobble of the parcel trajectories to limit our analysis to a single latitude band centered at 72°S. We also adopted a coordinate system in which variability introduced by adiabatic atmospheric motion is minimized. Specifically we calculated O_3 loss rates on each of ten isentropic surfaces scanned by the aircraft. Because our objective was to characterize the rate of O_3 destruction in the vortex as a whole, we selected the point of greatest penetration by the aircraft. This segment of the flight trajectory also provides vertical soundings and thus gives a detailed analysis of the altitude dependence of O_3 destruction (Fig. 2). Typically, a volume element circumscribes a complete trajectory in 4 to 6 days; therefore, a series of ten flights over a period of 31 days spans approximately six periods of circumpolar motion.

We compared observed O_3 loss rates with those predicted by halogen catalysis using low-order polynomial fits of observed O_3, ClO, and BrO concentrations versus time. Companion measurements of pressure and temperature were used to define the isentropic surfaces. Knowledge of solar zenith angles versus time for the 72°S latitude band provided the input needed to calculate exposure time in each diurnal cycle. Recent advances in understanding the kinetics of these radical-dimer catalytic processes complete the array of input data.

Recent laboratory studies are critical to our analysis. For Mechanism I, it is possible to convert in situ observations of ClO directly to O_3 destruction rates if (and only if) this mechanism is rate limiting and the reaction rate constant, k_1, is known for the appropriate temperature and pressure. Mechanism I is rate limiting if (i) the dominant isomer formed in the reaction of ClO with itself is the symmetric peroxy structure ClOOCl; (ii) photolysis of that structure yields two Cl atoms directly or by the photolysis products Cl + ClOO followed by thermal decomposition of ClOO; and (iii) thermal decomposition of Cl_2O_2 is slow relative to photolysis. If, for example, the product of ClO self reaction is the asymmetric form

ClOClO, and photolysis of that structure yields Cl + OClO, then the catalytic cycle would be terminated because OClO photolysis yields an O atom that would regenerate O_3.

A quantitative analysis of O_3 loss rates is now possible because (i) studies defining k_1 over the appropriate pressure-temperature regime have been reported (*33*); (ii) the detailed structure of the ClO dimer has been determined (*34*) with millimeter-wave emission techniques in conjunction with refined laboratory sources optimized for dimer formation; (iii) laboratory quantum-yield measurements of Cl-atom production from ClOOCl dimer photolysis at wavelengths appropriate to photodecomposition in the stratosphere have been carried out (*35*) and demonstrate that two Cl atoms are produced for each ultraviolet photon absorbed; and (iv) a full simulation of the temperature, pressure, and flow-velocity regime in which the ClO-BrO instrument operates has been completed. At pressures corresponding to 18 km these simulations result in absolute ClO concentrations 20% higher than values reported earlier (*29*) at the low temperatures encountered during the early stages of the Antarctic flight series. Flights after the end of August are unaffected at high altitude. At the low-temperature, high-pressure extremes encountered near the bottom of the dive segments of the flights, our ClO concentrations are 75% higher than those reported earlier as a result of the full laboratory simulation of flight conditions.

Our objective is to use the in situ observations in such a way that the analysis is simple enough to be derived from first principles yet reflects properly the context of current experimental uncertainties, of which there are three. First, there is the uncertainty associated with the reported absolute concentration of ClO and BrO, ±25% and ±35%, respectively, at 90% confidence limits. Second, there are uncertainties in the appropriate rate constants, k_1 and k_2, which are in both cases ±15%. Third, there is an uncertainty of ±15% associated with the assumption that the trajectories oscillate about the 72°S latitude belt and effectively average out varying ultraviolet exposure times.

We are thus left with analytical uncertainties evenly distributed among three categories: observed radical concentrations, laboratory determination of reaction rate constants, and variations in effective exposure times during diurnal periods. These lead to an uncertainty of ±35% in the determination of O_3 loss. This uncertainty is considerably larger than what we judge to be the contribution from dynamic exchange into and out of the CPR during the course of this experimental series.

In a ten-level analysis between 18.5 (450 K) and 13 km (360 K) (summarized in Fig. 6), we find that 75% of the observed O_3 loss rate is accounted for by Mechanism I alone and that the sum of Mechanisms I and II constitutes a catalytic destruction rate commensurate with observed ozone destruction rates.

A similar analysis of Mechanisms III and IV indicates that each of these processes constitutes a loss rate approximately 5% of the observed loss rate of ozone. Although we have considerable confidence in the simple steady-state relationship converting observed O_3 concentrations to $O(^3P)$ densities used in the quantitative analysis of Mechanism IV, we employed an upper limit of 1 pptv for the mixing ratio of HO_2 for Mechanism III.

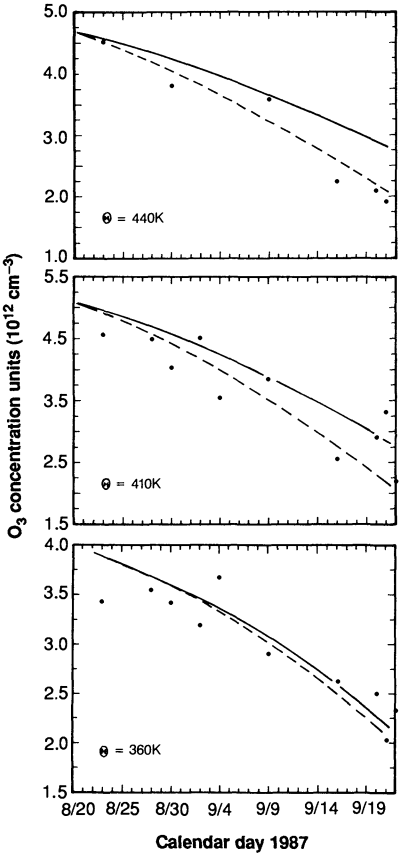

Fig. 6. Comparison between the observed disappearance of O_3 over the 4-week period of the mission and the calculated amount of ozone removed, based on simultaneously observed concentrations of ClO and BrO for two catalytic cycles. Mechanism I (solid line) and the most recent laboratory determination of the reaction rate constant for the rate-limiting step, and the sum of Mechanism I and Mechanism II (dashed line), which couple chlorine and bromine.

Summary

What sets Antarctic O_3 depletion apart in the context of global change is both the severity of the phenomenon and the unusual decoupling of physical and chemical time constants that control transformation rates in a specific region of the atmosphere. We (*36*) have presented a case in three parts based upon simultaneous, in situ observations of ClO, BrO, and O_3 concentrations designed to test catalytic processes coupling CFC release, which has elevated the stratospheric mixing ratio of chlorine from ~1 ppb in 1950 to ~3 ppb in 1990, to ozone depletion over Antarctica. When taken independently, each element in the case contains a segment of the puzzle that in itself is not conclusive. When taken together, however, they provide convincing evidence that the dramatic reduction in column-integrated O_3 over the Antarctic continent would not have occurred had CFCs not been synthesized and then added to the atmosphere.

REFERENCES AND NOTES

1. U.S. Committee for an International Geosphere-Biosphere Program, National Research Council, *Global Change in the Geosphere-Biosphere: Initial Priorities for an IGBP* (National Academy Press, Washington, DC, 1986); Board on Atmospheric Sciences and Climate and the Committee on Global Change Commission on Physical Sciences and Resources, National Research Council, *Ozone Depletion, Greenhouse Gases, and Climate Change* (National Academy Press, Washington, DC, 1989).
2. J. C. Farman, B. G. Gardiner, J. D. Shankin, *Nature* **315**, 207 (1985).
3. R. S. Stolarski *et al.*, *ibid.* **322**, 808 (1986).
4. T. Deshler, D. J. Hofmann, J. V. Hereford, C. B. Sutter, *Geophys. Res. Lett.* **17**, 151 (1990).
5. K. K. Tung, *ibid.* **13**, 13 (1986).
6. L. C. Callis and M. Natarajan, *J. Geophys. Res.* **91**, 771 (1986).
7. M. J. Molina and F. S. Rowland, *Nature* **249**, 810 (1974).
8. L. T. Molina and M. J. Molina, *J. Phys. Chem.* **91**, 433 (1987).
9. M. B. McElroy, R. J. Salawitch, S. C. Wofsy, J. A. Logan, *Nature* **321**, 759 (1986).
10. S. Solomon, R. R. Garcia, F. S. Rowland, D. J. Wuebbles, *ibid.*, p. 755.
11. D. J. Hofmann, *Rev. Geophys.* **26**, 113 (1988).
12. S. Solomon, G. H. Mount, R. W. Sanders, A. L. Schmeltekopf, *J. Geophys. Res.* **92**, 8329 (1987).
13. G. H. Mount, R. W. Sanders, A. L. Schmeltekopf, S. Solomon, *ibid.*, p. 8320.
14. R. L. deZafra, M. Jaramillo, A. Parrish, P. Solomon, J. Barrett, *Nature* **328**, 408 (1987); P. M. Solomon *et al.*, *ibid.*, p. 411.
15. C. B. Farmer, G. C. Toon, P. W. Schaper, J.-F. Blavier, L. L. Lowes, *ibid.* **329**, 126 (1987).
16. The Airborne Antarctic Ozone Experiment (AAOE) was organized by R. T. Watson as a multiagency operation involving the National Aeronautics and Space Administration (NASA), the National Oceanographic and Atmospheric Administration (NOAA), the National Science Foundation (NSF), and the Chemical

Manufacturer's Association (CMA) with A. F. Tuck, Project Scientist. An in-depth analysis of the results from AAOE mission, as well as the NOZE II series, appears in a special issue of *J. Geophys. Res.* **94**, 11,181 (1989).
17. A series of papers trace this development: J. G. Anderson, J. J. Margitan, D. H. Stedman, *Science* **198**, 501 (1977); J. G. Anderson, H. J. Grassl, R. E. Shetter, J. J. Margitan, *J. Geophys. Res.* **85**, 2869 (1980); J. J. Schwab and J. G. Anderson, *J. Quant. Spectrosc. Rad. Transfer* **27**, 445 (1982); W. H. Brune and J. G. Anderson, *Geophys. Res. Lett.* **13**, 1391 (1986); W. H. Brune, E. M. Weinstock, J. G. Anderson, *ibid.* **15**, 144 (1988).
18. See the discussion in W. H. Brune, J. G. Anderson, K. R. Chan, *J. Geophys. Res.* **94**, 16,639 (1989); *ibid.*, p. 16,649; D. W. Toohey, J. G. Anderson, W. H. Brune, K. R. Chan, *Geophys. Res. Lett.* **17**, 513 (1990).
19. M. H. Proffitt *et al.*, *J. Geophys. Res.* **94**, 16,547 (1989).
20. Potential temperature is defined by and computed from the expression $\theta = T(P_S/P)^x$, where T is the observed temperature of the air parcel, P_S is the surface pressure, P is the actual pressure of the air parcel, and x is the ratio of the gas constant, R, to the specific heat at constant pressure, C_p. A heuristic definition of potential temperature is that it is the temperature of an air parcel brought adiabatically from the point of interest to sea level.
21. For a complete discussion of the dynamics of polar vortices and a discussion of dynamical exchange, see M. R. Schoeberl and D. L. Hartmann, *Science* **251**, 46 (1991).
22. D. W. Fahey *et al.*, *J. Geophys. Res.* **94**, 16,665 (1989).
23. J. R. Podolske, M. Loewenstein, S. E. Strahan, K. R. Chan, *ibid.*, p. 16,767; L. E. Heidt, J. F. Vedder, W. H. Pollock, R. A. Lueb, B. E. Henry, *ibid.*, p. 11,599.
24. K. K. Kelly *et al.*, *ibid.*, p. 11,317.
25. J. G. Anderson, W. H. Brune, M. H. Proffitt, *ibid.*, p. 11,465.
26. O. B. Toon, P. Hamill, R. P. Turco, J. Pinto, *Geophys. Res. Lett.* **13**, 1284 (1986); P. J. Crutzen and F. Arnold, *Nature* **324**, 651 (1986); M. B. McElroy, R. J. Salawitch, S. C. Wofsy, *Geophys. Res. Lett.* **13**, 1296 (1986); L. R. Poole and M. P. McCormick, *J. Geophys. Res.* **93**, 8423 (1988).
27. M. J. Molina, T. Tso, L. T. Molina, F. C. Y. Wang, *Science* **238**, 1253 (1987); M. A. Tolbert, M. J. Rossi, R. Malhotra, D. M. Golden, *ibid.*, p. 1258.
28. M. R. Schoeberl *et al.*, *J. Geophys. Res.* **94**, 16,815 (1989).
29. J. G. Anderson *et al.*, *ibid.*, p. 11,480.
30. The opposing views on whether the antarctic vortex more nearly approximates (i) an isolated air mass or (ii) a flow reactor are represented, respectively, by (i) D. L. Hartmann *et al.*, *J. Geophys. Res.* **94**, 16,779 (1989); M. R. Schoeberl *et al.* (*28*); and (ii) A. F. Tuck *et al.*, *ibid.*, p. 11,687; M. J. Proffitt *et al.*, *ibid.*, p. 16,797; E. F. Danielsen, *J. Atmos. Sci.*, **47**, 2013 (1990).
31. M. H. Proffitt, D. W. Fahey, K. K. Kelly, A. F. Tuck, *Nature* **342**, 233 (1989).
32. D. E. Anderson and S. A. Lloyd, *J. Geophys. Res.* **95**, 7429 (1990); D. E. Anderson, *Planet. Space Sci.* **31**, 1517 (1983).
33. S. P. Sander, R. R. Friedl, Y. L. Yung, *Science* **245**, 1095 (1989); M. Trolier, R. L. Mauldin III, A. R. Ravishankara, *J. Phys. Chem.* **94**, 4896 (1990).
34. M. Birk *et al.*, *J. Chem. Phys.* **91**, 6588 (1989).
35. M. J. Molina, A. J. Colussi, L. T. Molina, R. N. Schindler, T.-L. Tso, *Chem. Phys. Lett.* **173**, 310 (1990).
36. R. Watson was primarily responsible for organizing and expediting the Airborne Antarctic Ozone Experiment (AAOE). A. Tuck orchestrated the ER-2 and DC-8 operations, the aircraft trajectory, the British Meteorology Office weather forecasts, and the science meetings in Punta Arenas, Chile, during the mission. Field support for this mission came both from the NOAA Aeronomy Lab staff, notably T. Thompson and R. Winkler, and from the NASA Ames staff led by E. Condon and G. Ferry. We also thank N. Hazen and J. Demusz for the optical-mechanical and electronic design of the instrument, and N. Allen and M. Mueller, who developed the software for both the flight system and data reduction. P. Soderman played a critical role in the conception of the double-ducted arrangement used in the experiment. A. Schmeltekopf gave us invaluable advice. B. Ferguson helped with the ER-2 aircraft. We also thank J. Arveson and J. Barrilleaux. Finally, we thank the pilots: R. Williams, J. Hoyt, J. Barrilleaux, and D. Krumrey. Research was supported by NASA contract NASW 3960 and NAG2-443.

The Dynamics of the Stratospheric Polar Vortex and Its Relation to Springtime Ozone Depletions

MARK R. SCHOEBERL AND DENNIS L. HARTMANN

Dramatic springtime depletions of ozone in polar regions require that polar stratospheric air has a high degree of dynamical isolation and extremely cold temperatures necessary for the formation of polar stratospheric clouds. Both of these conditions are produced within the stratospheric winter polar vortex. Recent aircraft missions have provided new information about the structure of polar vortices during winter and their relation to polar ozone depletions. The aircraft data show that gradients of potential vorticity and the concentration of conservative trace species are large at the transition from mid-latitude to polar air. The presence of such sharp gradients at the boundary of polar air implies that the inward mixing of heat and constituents is strongly inhibited and that the perturbed polar stratospheric chemistry associated with the ozone hole is isolated from the rest of the stratosphere until the vortex breaks up in late spring. The overall size of the polar vortex thus limits the maximum areal coverage of the annual polar ozone depletions. Because it appears that this limit has not been reached for the Antarctic depletions, the possibility of future increases in the size of the Antarctic ozone hole is left open. In the Northern Hemisphere, the smaller vortex and the more restricted region of cold temperatures suggest that this region has a smaller theoretical maximum for column ozone depletion, about 40 percent of the currently observed change in the Antarctic ozone column in spring.

THE STRATOSPHERE IS THE ATMOSPHERIC REGION JUST above the tropopause, between roughly 12 and 50 km (100 and 1 mb in pressure). Within this region the air temperature generally increases with altitude rising from −50°C or lower at the tropopause to greater than −20°C at 50 km. The relative warmth of the stratosphere results from the absorption of solar ultraviolet radiation by O_3, which has its highest mixing ratio in the stratosphere. This heating by solar absorption is balanced by cooling through emission of thermal infrared radiation, primarily from the 15-μm band of CO_2. After the autumnal equinox, the polar regions fall into darkness and the solar ultraviolet heating ceases. Emission of thermal radiation quickly cools the polar stratosphere to temper-